arXiv:1703.03689v1 [cond-mat.mes-hall] 10 Mar 2017

Ultrafast and energy-efficient spin manipulation: Antiferromagnetism beats ferromagnetism

Nele Thielemann-Kühn,[1,2,*] Daniel Schick,[1] Niko Pontius,[1] Christoph Trabant,[1,2,3] Rolf Mitzner,[1] Karsten Holldack,[1] Hartmut Zabel,[4] Alexander Föhlisch,[1,2] and Christian Schüßler-Langeheine[1]

[1]*Institut für Methoden und Instrumentierung der Forschung mit Synchrotronstrahlung, Helmholtz-Zentrum Berlin für Materialien und Energie GmbH, Albert-Einstein-Straße 15, 12489 Berlin, Germany*

[2]*Institut für Physik und Astronomie, Universität Potsdam, Karl-Liebknecht-Straße 24/25, 14476 Potsdam, Germany*

[3]*II. Physikalisches Institut, Universität zu Köln, Zülpicher Straße 77, 50937 Köln, Germany*

[4]*Institut für Physik, Johannes-Gutenberg-Universität Mainz, Staudingerweg 7, 55128 Mainz, Germany*

(Dated: March 13, 2017)

Abstract

By comparing femtosecond laser pulse induced ferro- and antiferromagnetic dynamics in one and the same material - metallic dysprosium - we show both to behave fundamentally different. Antiferromagnetic order is considerably faster and much more efficiently manipulated by optical excitation than its ferromagnetic counterpart. We assign the fast and extremely efficient process in the antiferromagnet to an interatomic transfer of angular momentum within the spin system. Our findings do not only reveal this angular momentum transfer channel effective in antiferromagnets and other magnetic structures with non-parallel spin alignment, they also point out a possible route towards energy-efficient spin manipulation for magnetic devices.

Striving for novel concepts for faster and more energy-efficient data processing and storage, a wealth of experimental and theoretical studies in the field of ultrafast magnetic dynamics has been carried out [1–14]. This brought the understanding that a speed limit for spin manipulation is governed by the achievable angular momentum transfer. For any change of magnetic order fundamental conservation laws require transfer of angular momentum associated with the atomic magnetic moments [1, 15]. This is particularly relevant when magnetic order is to be affected on ultra-short time scales, e.g., by femtosecond laser pulse excitation. Here angular momentum transfer effectively limits the speed of magnetic manipulation. Various transfer channels have been identified including local scattering processes [2–5] as well as spin transport [6–9], and their relative importance for ultrafast magnetic dynamics is subject of intense debate [1, 3, 10–12]. Manipulating ferromagnetic order via local processes requires angular momentum transfer out of the spin system into an external reservoir like the lattice. In contrast, manipulation of antiferromagnetic order with vanishing net magnetization, could be achieved by redistribution of angular momentum within the spin system itself; transfer of angular momentum into other degrees of freedom is not required. One would therefore expect any change of antiferromagnetic order to occur faster than modifications of ferromagnetic order.

So far, antiferromagnetic dynamics was mostly studied experimentally in transition-metal oxides and it was found to proceed over a wide range of time scales including ultrafast dynamics within 230 fs [16], but also much slower dynamics on picosecond time scales [17]. In ferrimagnetic metallic alloys of $3d$ and $4f$ metals, ultrafast angular momentum transfer between antiferromagnetically exchange-coupled sublattices was observed [13, 18]. These results, however, are not straightforwardly comparable to the wealth of work about ferromagnetic metals: for $3d$-$4f$ alloy dynamics static inhomogeneity has been shown to play a crucial role [19]; and in oxides the exchange coupling mechanisms are different to those in metals. This renders quantitative comparison with the thoroughly studied elemental ferromagnets ambiguous. Already within one material class any magnetic dynamics - ferromagnetic as well as antiferromagnetic - is expected to depend on the size of the magnetic moment [20] and on material properties like the spin-orbit, spin-lattice and electron-lattice interaction [1]. To avoid such complications, we compare ferromagnetic and antiferromagnetic dynamics in the most direct way in one and the same material: metallic dysprosium (Dy).

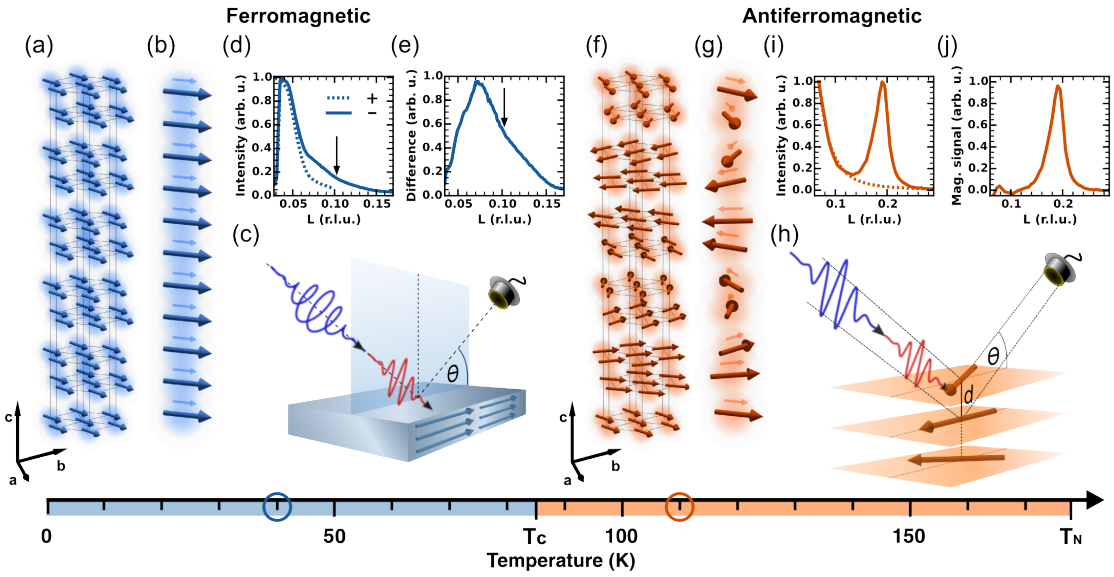

FIG. 1: (a-b) Ferromagnetic spin structure of the $4f$ (large arrows) and $5d$ spins (small arrows). (c) Geometry for probing ferromagnetism with circularly polarized soft x-rays tuned to the Dy M_5 resonance; a near-infrared laser pulse is shown as red wave packet. (d) Specular reflectivity vs. momentum transfer, L, for opposite photon helicities (solid and dashed lines). The difference (e) is the ferromagnetic contrast and the temporal response is probed at the momentum transfer value marked by the arrow. (f-g) Antiferromagnetic spin structure. (h) Geometry for probing antiferromagnetic order with linearly polarized soft x-rays. (i) Magnetic Bragg peak due to the magnetic helix period length (about 5 times the crystalline unit cell or 10 atomic layers) and a weak reflectivity background (dashed line) that has been subtracted in (j). For visual clarity the lateral offset between Dy sites in neighboring layers has been omitted in (b) and (g).

Dy is ferromagnetic at low temperatures and has a helical antiferromagnetic phase between 85 K and 178 K [21], see Fig. 1. The strongly localized $4f$ magnetic moments (10 μB per atom) are magnetically coupled by indirect (RKKY) exchange through intra-atomic spin-polarization of mostly $5d$ states in the ($5d6s$) conduction band [22, 23]. In the ferromagnetic phase all $4f$ and $5d$ spins are parallel aligned within the basal ab-planes, see Fig. 1 (a,b). In the antiferromagnetic phase the $4f$ spins within each ab-plane remain ferromagnetically aligned but form an helical structure along the crystallographic c-axis, see Fig. 1 (f,g).

Ferro- and antiferromagnetic $4f$ order can straightforwardly be probed with soft x-rays

tuned to the $3d \rightarrow 4f$ electronic excitation (M_5-edge at around 1292 eV photon energy). For ferromagnetic order we used magnetic circular dichroism (MCD) in reflection geometry [24, 25], *i.e.*, the effect that a ferromagnetic sample reflects elliptically polarized x-rays differently depending on the photon helicity projection onto the sample magnetization. For probing ferromagnetic dynamics the sample was held at 40 K. The specular reflected intensity at the maximum of the Dy M_5 absorption edge was recorded for opposite sign of a magnetic field of 80 mT oriented in the scattering plane and parallel to the sample surface. Incidence and detection angles were set to 5 degrees with respect to the sample surface. In order to determine the ferromagnetic order parameter the difference in reflected intensities for opposite direction of the magnetic field was taken [24].

Antiferromagnetic order was studied by resonant magnetic x-ray diffraction: The helical magnetic order leads to a superstructure Bragg peak [26] at $(0\ 0\ \tau)$ with $\tau \approx 0.19$ in reciprocal lattice units (r.l.u.). The antiferromagnetic phase data were recorded using linearly polarized x-rays with the sample held at 110 K. The magnetic diffraction peak at $(0\ 0\ \tau)$ occurs in specular geometry with an incidence angle of about 9.5 degrees with respect to the sample surface. In order to determine the antiferromagnetic order parameter the square root of scattering signal was calculated [27].

Since resonant magnetic x-ray diffraction and magnetic circular dichroism are based on exactly the same contrast mechanism [28], a combination of both techniques allows for determining the ferro- and antiferromagnetic order parameters in a directly comparable way. For an overview of experimental geometries and data acquisition see Fig. 1. As sample we chose a 120 nm thin metallic Dy film grown by molecular beam epitaxy with (0 0 1) surface orientation. The film was sandwiched between Yttrium (Y) layers to minimize strain; Niobium (Nb) served as buffer layer and oxidation protection; sapphire was the substrate [29]. The stacking in the film was Nb (2.5 nm) / Y (3 nm) / Dy (120 nm) / Y (70 nm) / Nb (50 nm) / *a*-plane sapphire.

The experiment was carried out at the FemtoSpeX slicing facility at the electron storage ring BESSY II of the Helmholtz-Zentrum Berlin [30]. Magnetic dynamics was induced by 800 nm-near-infrared-laser pulses of 50 fs duration. The magnetic signal was probed with 100 fs x-ray pulses, hitting the sample with 6 kHz repetition rate, while the pump laser was operated at 3 kHz such that alternating signals with and without pump laser excitation were detected. The latter were used for normalization. Detailed information on the experimental

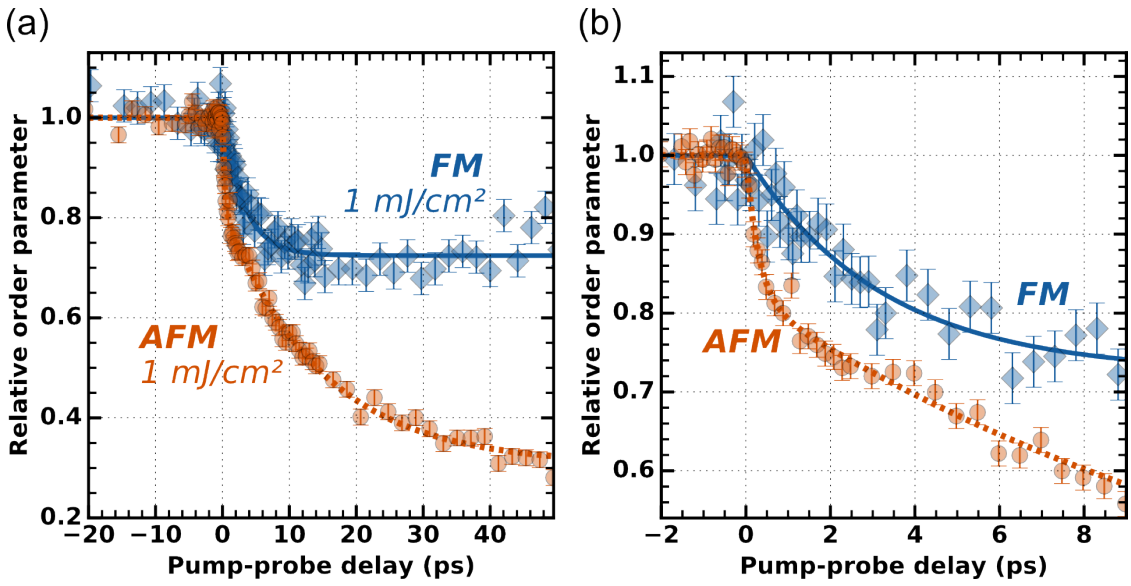

FIG. 2: (a) Pump-probe delay scans in the ferromagnetic (blue) and antiferromagnetic (orange) phase for an absorbed laser fluence of 1 mJ/cm^2. The symbols denote the normalized magnetic order parameter; the lines denote exponential fits to the data. (b) First 9 ps of the delay traces on an enlarged scale.

setup, data acquisition, data analysis, as well as the complete set of evaluated data can be found in the supplemental material.

Typical dynamical data are presented in Fig. 2 (a). The two transients demonstrate the clearly different response of the two order parameters. After an equally strong laser excitation (absorbed fluence), both magnetic order parameters are reduced, but the quenching of the antiferromagnetic order is considerably and consistently stronger for all delays. Moreover, the shapes of the two transients are significantly different. Zooming into the first 9 ps [Fig. 2 (b)] reveals the initial antiferromagnetic order parameter loss to occur much faster than its ferromagnetic counterpart. For antiferromagnetic dynamics we find an initial fast reduction with an exponential time constant of (290 ± 40) fs followed by a slower one of (14 ± 1) ps. In contrast, the ferromagnetic dynamics occurs with a single time constant of (3.2 ± 0.3) ps. The solid lines in Fig. 2 (a,b) show results of least square fits to double or single exponential decay models (see supplemental materials).

A fluence dependent investigation, see Fig. 3 (a), shows the initial antiferromagnetic decay time constant to vary very little for low absorbed fluences up to 1.2 mJ/cm^2 with an average value of (220 ± 70) fs. For higher fluences, the decay becomes slower reading 1040 fs

for the highest fluence considered in this work. Remarkably, all initial antiferromagnetic dynamics are significantly faster than the single time constants in the ferromagnetic phase, which on average amount to (6 ± 2) ps [Fig. 3 (a)]. The difference between ferromagnetic and antiferromagnetic dynamics becomes even more pronounced comparing the momentary rate of atomic angular momentum transfer [Fig. 3 (b)]. We define the (momentary) angular momentum transfer rate as the change of the magnetic order parameter per time. The maximum transfer rate in the antiferromagnetic phase is more than five times higher than in the ferromagnetic phase. This trend is true for a wide range of laser excitation fluences. In Fig. 3 (c) we present the maximum measured angular momentum transfer rate vs. the absorbed laser fluence. The maximum antiferromagnetic transfer rates are always higher by a factor of four to five. Ultrafast spin manipulation in the antiferromagnet is hence more energy-efficient than in the ferromagnet.

We note that in between the base temperatures of the experiments (40 K and 110 K, respectively) the static order parameter changes by less than 15 %. This small change can not cause such different magnetic dynamics. Both temperatures are also well below the highest ordering temperature of 178 K. We can hence exclude an influence of critical effects close to the paramagnetic phase transition on the dynamics. The higher energy efficiency along with the faster spin manipulation for the antiferromagnetic phase is a true consequence of the different spin structures.

In the following we discuss the angular momentum transfer channels responsible for the observed behavior. We assign the difference between ferromagnetic and antiferromagnetic dynamics for short delay times to an angular momentum transfer channel only effective in magnetic systems like antiferromagnets, i.e., where spin orientations are not parallel. This transfer channel essentially bases on interatomic spin hopping.

Since a direct excitation of $4f$ electrons (3.8 eV binding energy) or a transition of $5d6s$ electrons into unoccupied $4f$ states (2 eV above Fermi level) is not possible in both magnetic phases with the pump photon energy of 1.5 eV [31], the pump laser pulse essentially excites delocalized $5d6s$ electrons. In the antiferromagnetic phase these excited electrons with their spins initially aligned parallel to the local $4f$ spins hop to adjacent sites with non parallel $4f$ spins. This brings about a disordering of the $5d$ spin subsystem. Subsequently this disorder is imposed onto the $4f$ subsystem via the strong $4f - 5d$ coupling [14]. Note that such interatomic spin transfer also occurs in the ferromagnetic phase but - owing to the allover

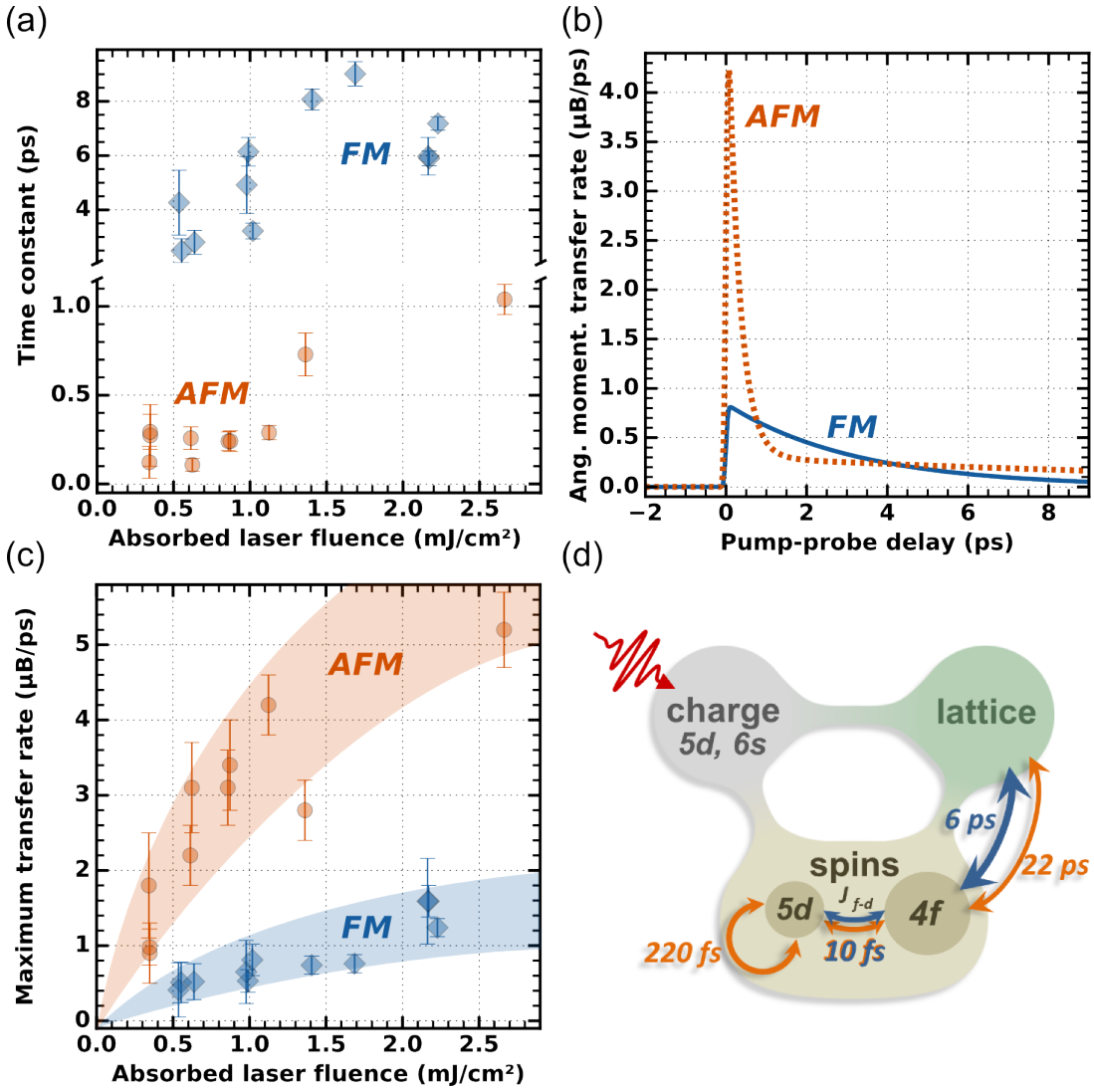

FIG. 3: (a) Short time constants for the antiferromagnetic and single time constants for the ferromagnetic dynamics, determined from the delay traces for different absorbed laser fluences (note broken y-axis). (b) The momentary rate of average atomic angular momentum transfer derived from the exponential fits in Fig. 2 (a). (c) Maximum momentary angular momentum transfer rate deduced from the delay traces for different absorbed laser fluences. The shaded areas are guides to the eye. (d) Channels of angular momentum transfer active in the antiferromagnetic (orange arrows) and ferromagnetic (blue arrows) phase of Dy, see text.

parallel spin-alignment - will not cause any demagnetization and has therefore not been observed in ferromagnetic dynamics studies.

For discussing the ferromagnetic case it is instructive to compare Dy with the neighboring

lanthanide ferromagnet terbium (Tb), which has a very similar electronic structure. For Tb, two different channels transferring angular momentum from $4f$ electrons to the lattice have been identified: i) via fast intra-atomic exchange with the delocalized $5d$ valence electrons in the presence of hot electrons and ii) the slower direct $4f$ spin lattice coupling [14]. Interestingly, the fast decay channel i) is not found in our Dy ferromagnetic data. Since structural and magnetic properties of Dy and Tb are very similar, major differences in $4f-5d$ or $4f$-lattice coupling are not to be expected. A main difference between the Tb experiment in Ref. 14 and our Dy experiment is the sample thickness, though: The Tb film in Ref. 14 was 10 nm thick; while our Dy sample had a thickness of 120 nm [32]. It is to be expected that variation of the film thickness in this range (10 nm are 35 monolayers) neither affects the $4f-5d$ nor the $4f$-lattice coupling. On the other hand, spin transport, should strongly depend on the sample dimensions as it involves spin currents into non-magnetic regions [6]. For our thick Dy film only the very thin non-magnetic cap layer is near the probed volume while the thick non-magnetic Y buffer layer is far away from the photoexcited regions. We therefore speculate that the fast time constant seen before in Tb may actually not be due to channel i) but rather be caused by spin transport.

We would like to stress that the question about the existence of channel i) in ferromagnetic Dy does not affect our conclusion about the interatomic spin transfer being fast and energy efficient: even if we missed a fast ferromagnetic transfer channel in our Dy sample, this channel can be expected to have a similar time constant as the one in Tb. For the latter (740 ± 250) fs was found [14, 33], which is still much slower than our result for the fast antiferromagnetic dynamics in Dy.

Coming back to the second, slower antiferromagnetic dynamics with a time constant of (22 ± 7) ps: this and the ferromagnetic time constant of (6 ± 2) ps are of similar order of magnitude as the time constant in Tb (8 ps) related to the $4f$-spin-lattice coupling [channel ii)] and should have the same origin. The quantitative difference we find between the two Dy phases hint to stronger $4f$-lattice coupling in the ferromagnetic phase [34], which agrees with the observation that in ferromagnetic Dy the $4f$ spins are confined by a uniaxial in-plane anisotropy which is absent in the antiferromagnetic phase [22].

In Fig. 3 (d) we present an overview of the different angular-momentum transfer channels with their characteristic time scales, including the interatomic spin transfer channel. In antiferromagnetic Dy the interatomic transfer channel via hopping of $5d$ electrons to adjacent

atomic sites is effective in addition to those channels available in the ferromagnetic phase. The opening of this channel leads to an up to 30 times faster reduction of the magnetic order compared to the ferromagnetic phase. For the $4f-5d$ coupling we refer to the value of 10 fs following Ref. 23 [35].

Our case study on Dy shows that for a given material spin manipulation is much faster and more energy-efficiently achieved when spins are antiferromagnetically aligned compared to ferromagnetic spin order. Generally any non-parallel spin alignment would allow to redistribute angular momentum within the spin system. Since in the helical phase of Dy the angle between neighboring spins is only of the order of 34 degrees, even stronger effects may occur for larger relative angles. Our results apply primarily to $4f$ metals but equivalent behavior should be found in other $4f$ materials. Since the angular momentum redistribution occurs in the case of Dy through the $5d$ electrons even $3d$ antiferromagnets can be expected to show faster dynamics and/or higher energy efficiency than their ferromagnetic counterparts.

The highly efficient ultrafast interatomic transfer of angular momentum between non parallel spins may define a route towards more energy-efficient ultrafast spin manipulation in devices. Non parallel coupled magnetic moments may serve as spin sinks that reduce the energy required to manipulate spin order or allow for tuning time constants. The all optical switching in, e.g., GdFeCo occurs via an almost complete quenching of the magnetization in the material [18]. Most of the angular momentum needs to be transferred out of the $4f$ system before switching sets in. Based on our finding, the energy needed to reach this transfer should be much lower when antiparallel $4f$ spins are available either within the same material or possibly even in a multilayer structure. Clever material design can make use of this effect to reduce the energy needed for ultrafast spin manipulation like optically induced magnetic switching.

N.T.-K., D.S., N.P., C.T., H.Z. and C.S.-L. planned and carried out the experiment with experimental support from R.M. and K.H.; H.Z. prepared the sample; N.T.-K., D.S. and N.P. analyzed the data; N.T.-K., N.P., D.S. and C.S.-L. wrote the manuscript with help from the other authors.

Funding: Work was supported by the BMBF (contract 05K10PK2). D.S. acknowledges the Helmholtz Association for funding via the Helmholtz Postdoc Program PD-142. N.T.-K. acknowledges the Helmholtz Association for funding via the Helmholtz Virtual Institute "Dynamic Pathways in Multidimensional Landscapes".

* Electronic address: nele.thielemann@helmholtz-berlin.de

[1] A. Kirilyuk, A. V. Kimel, and T. Rasing, Rev. Mod. Phys. **82**, 2731 (2010), ISSN 00346861.

[2] D. Steiauf and M. Fähnle, Phys. Rev. B **79**, 140401 (2009), ISSN 1098-0121.

[3] B. Koopmans, G. Malinowski, F. Dalla Longa, D. Steiauf, M. Fähnle, T. Roth, M. Cinchetti, and M. Aeschlimann, Nat. Mater. **9**, 259 (2010), ISSN 1476-1122.

[4] A. J. Schellekens and B. Koopmans, Phys. Rev. Lett. **110**, 217204 (2013), ISSN 0031-9007.

[5] B. Y. Mueller, T. Roth, M. Cinchetti, M. Aeschlimann, and B. Rethfeld, New J. Phys. **13**, 123010 (2011), ISSN 1367-2630, 1108.5170.

[6] M. Battiato, K. Carva, and P. M. Oppeneer, Phys. Rev. Lett. **105**, 027203 (2010), ISSN 0031-9007.

[7] G. Malinowski, F. Dalla Longa, J. H. H. Rietjens, P. V. Paluskar, R. Huijink, H. J. M. Swagten, and B. Koopmans, Nat. Phys. **4**, 855 (2008), ISSN 1745-2473.

[8] D. Rudolf, C. La-O-Vorakiat, M. Battiato, R. Adam, J. M. Shaw, E. Turgut, P. Maldonado, S. Mathias, P. Grychtol, H. T. Nembach, et al., Nat. Commun. **3**, 1037 (2012), ISSN 2041-1723.

[9] A. Eschenlohr, M. Battiato, P. Maldonado, N. Pontius, T. Kachel, K. Holldack, R. Mitzner, A. Föhlisch, P. M. Oppeneer, and C. Stamm, Nat. Mater. **12**, 332 (2013), ISSN 1476-1122.

[10] S. Essert and H. C. Schneider, Phys. Rev. B **84**, 224405 (2011), ISSN 1098-0121.

[11] T. Roth, A. J. Schellekens, S. Alebrand, O. Schmitt, D. Steil, B. Koopmans, M. Cinchetti, and M. Aeschlimann, Phys. Rev. X **2**, 021006 (2012), ISSN 2160-3308.

[12] T. Ostler, J. Barker, R. Evans, R. Chantrell, U. Atxitia, O. Chubykalo-Fesenko, S. El Moussaoui, L. Le Guyader, E. Mengotti, L. Heyderman, et al., Nat. Commun. **3**, 666 (2012), ISSN 2041-1723, arXiv:1011.1669v3.

[13] N. Bergeard, V. López-Flores, V. Halté, M. Hehn, C. Stamm, N. Pontius, E. Beaurepaire, and C. Boeglin, Nat. Commun. **5**, 3466 (2014), ISSN 2041-1723.

[14] M. Wietstruk, A. Melnikov, C. Stamm, T. Kachel, N. Pontius, M. Sultan, C. Gahl, M. Weinelt, H. a. Dürr, and U. Bovensiepen, Phys. Rev. Lett. **106**, 127401 (2011), ISSN 0031-9007.

[15] A. Einstein and W. de Haas, Verhandl. Deut. Phys. Ges. **17**, 152 (1915).

[16] M. Fiebig, N. P. Duong, T. Satoh, B. B. Van Aken, K. Miyano, Y. Tomioka, and Y. Tokura, J. Phys. D. Appl. Phys. **41**, 164005 (2008), ISSN 0022-3727.

[17] R. I. Tobey, S. Wall, M. Först, H. Bromberger, V. Khanna, J. J. Turner, W. Schlotter, M. Trigo, O. Krupin, W. S. Lee, et al., Phys. Rev. B **86**, 064425 (2012), ISSN 1098-0121.

[18] I. Radu, K. Vahaplar, C. Stamm, T. Kachel, N. Pontius, H. A. Dürr, T. A. Ostler, J. Barker, R. F. L. Evans, R. W. Chantrell, et al., Nature **472**, 205 (2011), ISSN 0028-0836.

[19] C. E. Graves, A. H. Reid, T. Wang, B. Wu, S. de Jong, K. Vahaplar, I. Radu, D. P. Bernstein, M. Messerschmidt, L. Müller, et al., Nat. Mater. **12**, 293 (2013), ISSN 1476-1122.

[20] I. Radu, C. Stamm, A. Eschenlohr, F. Radu, R. Abrudan, K. Vahaplar, T. Kachel, N. Pontius, R. Mitzner, K. Holldack, et al., SPIN **05**, 1550004 (2015), ISSN 2010-3247.

[21] D. R. Behrendt, S. Legvold, and F. H. Spedding, Phys. Rev. **109**, 1544 (1958), ISSN 0031-899X.

[22] J. Jensen and A. R. Mackintosh, *Rare earth magnetism: structures and excitations*, International series of monographs on physics (Clarendon Press, 1991), ISBN 9780198520276.

[23] R. Ahuja, S. Auluck, B. Johansson, and M. S. S. Brooks, Phys. Rev. B **50**, 5147 (1994), ISSN 0163-1829.

[24] H.-C. Mertins, D. Abramsohn, A. Gaupp, F. Schäfers, W. Gudat, O. Zaharko, H. Grimmer, and P. M. Oppeneer, Phys. Rev. B **66**, 184404 (2002), ISSN 0163-1829.

[25] S. Macke and E. Goering, J. Phys. Condens. Matter **26**, 363201 (2014), ISSN 0953-8984.

[26] H. Ott, C. Schüßler-Langeheine, E. Schierle, E. Weschke, and G. Kaindl, Phys. Rev. B **82**, 214408 (2010), ISSN 1098-0121.

[27] H. Ott, C. Schüßler-Langeheine, E. Schierle, A. Grigoriev, V. Leiner, H. Zabel, G. Kaindl, and E. Weschke, Phys. Rev. B **74**, 094412 (2006), ISSN 1098-0121, URL `http://link.aps.org/doi/10.1103/PhysRevB.74.094412`.

[28] S. W. Lovesey and S. P. Collins, *X-Ray Scattering andAbsorption by Magnetic Materials* (Oxford University Press, Oxford, 1996), ISBN 9780198517375.

[29] V. Leiner, M. Ay, and H. Zabel, Phys. Rev. B **70**, 104429 (2004), ISSN 1098-0121.

[30] K. Holldack, J. Bahrdt, A. Balzer, U. Bovensiepen, M. Brzhezinskaya, A. Erko, A. Eschenlohr, R. Follath, A. Firsov, W. Frentrup, et al., J. Synchrotron Radiat. **21**, 1090 (2014), ISSN 1600-5775.

[31] S. Lebègue, A. Svane, M. I. Katsnelson, A. I. Lichtenstein, and O. Eriksson, J. Phys. Condens. Matter **18**, 6329 (2006), ISSN 0953-8984.

[32] Thin Dy films do not develop a ferromagnetic phase when epitaxially grown between Y layers.

[33] A. Eschenlohr, M. Sultan, A. Melnikov, N. Bergeard, J. Wieczorek, T. Kachel, C. Stamm, and U. Bovensiepen, Phys. Rev. B **89**, 214423 (2014), ISSN 1098-0121.

[34] W. Hübner and K. H. Bennemann, Phys. Rev. B **53**, 3422 (1996), ISSN 0163-1829.

[35] This value has recently been questioned when photoemission experiments and theory results found a slower $4f - 5d$ coupling for gadolinium (Gd) [36]. The authors of that study stress, however, that their results strongly depend on the low $4f - 5d$ overlap, which is a particular property of the Gd band structure. For Dy this overlap is larger. Furthermore, a recent magnetic diffraction study on $4f$ and $5d$ dynamics in antiferromagnetic holmium (similar $4f - 5d$ overlap as in Dy), also found a very efficient $4f - 5d$ coupling [37]. And even for Gd, theoretical predictions are diverse [38].

[36] B. Frietsch, J. Bowlan, R. Carley, M. Teichmann, S. Wienholdt, D. Hinzke, U. Nowak, K. Carva, P. M. Oppeneer, and M. Weinelt, Nat. Commun. **6**, 8262 (2015), ISSN 2041-1723.

[37] L. Rettig, C. Dornes, N. Thielemann-Kühn, N. Pontius, H. Zabel, D. L. Schlagel, T. A. Lograsso, M. Chollet, A. Robert, M. Sikorski, et al., Phys. Rev. Lett. **116**, 257202 (2016), ISSN 0031-9007, 1511.05315.

[38] L. M. Sandratskii, Phys. Rev. B **90**, 184406 (2014), ISSN 1098-0121.

arXiv:1703.03689v1 [cond-mat.mes-hall] 10 Mar 2017

Supplemental material for Ultrafast and energy-efficient spin manipulation: Antiferromagnetism beats ferromagnetism

Nele Thielemann-Kühn,[1,2,*] Daniel Schick,[1] Niko Pontius,[1] Christoph Trabant,[1,2,3] Rolf Mitzner,[1] Karsten Holldack,[1] Hartmut Zabel,[4] Alexander Föhlisch,[1,2] and Christian Schüßler-Langeheine[1]

[1] *Institut für Methoden und Instrumentierung der Forschung mit Synchrotronstrahlung, Helmholtz-Zentrum Berlin für Materialien und Energie GmbH, Albert-Einstein-Straße 15, 12489 Berlin, Germany*

[2] *Institut für Physik und Astronomie, Universität Potsdam, Karl-Liebknecht-Straße 24/25, 14476 Potsdam, Germany*

[3] *II. Physikalisches Institut, Universität zu Köln, Zülpicher Straße 77, 50937 Köln, Germany*

[4] *Institut für Physik, Johannes-Gutenberg-Universität Mainz, Staudingerweg 7, 55128 Mainz, Germany*

(Dated: March 13, 2017)

Contents

Antiferromagnetic signal 3

Ferromagnetic signal 5

Long exponential time constants 6

Data acquisition and treatment 6

Data analysis 8

Statistical Analysis 11

Angular momentum transfer rate 11

Pump fluence determination 12

References 14

ANTIFERROMAGNETIC SIGNAL

The antiferromagnetic order parameter was probed via the intensity of the magnetic Bragg peak at (0 0 τ). Figure S1 A shows the x-ray resonant diffraction spectrum in the vicinity of the Dy M_5 resonance, i.e. the energy dependence of the magnetic peak. The intensity of this antiferromagnetic diffraction peak is proportional to the squared order parameter, i.e. $I \propto M^2$ [1]. At 110 K the peak occurs at a momentum transfer of $\tau \approx 0.19$ reciprocal lattice units (r.l.u.) along the [0 0 1] (L) direction.

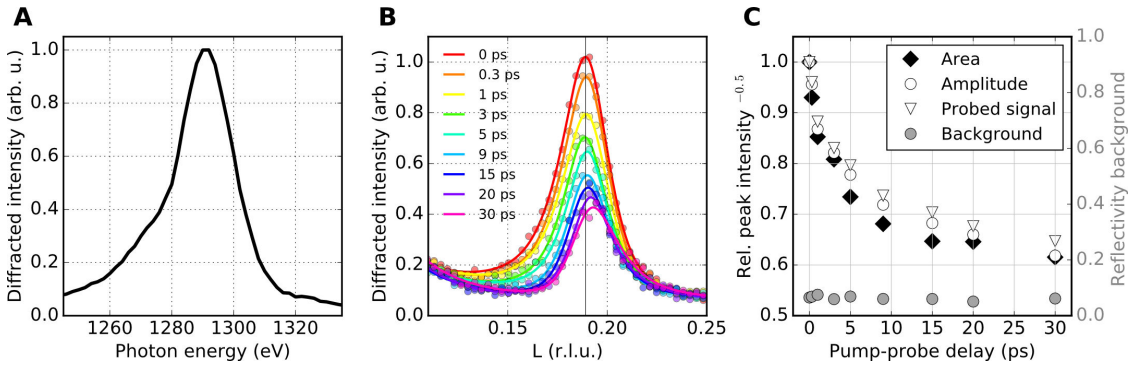

FIG. S1: Dynamics of the magnetic Bragg peak. (A) Resonant x-ray diffraction spectrum around the Dy M_5 edge recorded with linearly polarized x-rays. The energy was varied while keeping the momentum transfer fixed at (0 0 τ). The spectrum was recorded at the FemtoSpeX slicing facility at BESSY II with an energy resolution of $E/\Delta E \approx 500$. (B) Scans through momentum space along [001] (L) through the magnetic diffraction peak on the M_5 resonance for different pump-probe delays at an absorbed pump fluence of 1 mJ/cm^2. Upon photoexcitation the peak intensity is reduced. The position of the diffraction peak does not shift significantly for pump-probe delays below 15 ps. At larger delays a shift to larger momentum transfer occurs. The solid lines show the results of fits to the data. The fits assume a pseudo-Voigt peak profile on a reflectivity background. (C) Peak area and amplitude of the diffraction peak (minus reflectivity background), probed signal and reflectivity background at $\tau \approx 0.19$ for different pump-probe delays. The quantities are determined from the fits to the diffraction peak in (B).

The relation between L and scattering angle θ is:

$$L = \frac{2c}{\lambda} \sin\theta \tag{1}$$

with $c = 5.654$ Å being the (room-temperature) lattice constant and λ the photon wave-

length. For 1292 eV, $\lambda \approx 9.6$ Å. For antiferromagnetic Dy, the peak position in momentum space depends sensitively on the sample temperature. We therefore verified that the peak position (and peak width) does not change within the first 15 ps after photoexcitation (see Fig. S1 B) such that the peak amplitude is proportional to the peak area and thus uniquely linked to the temporal evolution of the magnetic order. For longer delays we see a small shift of the peak to larger momenta. Peak shifts caused by static heating scale with the laser pump fluence and were taken into account by aligning the momentum transfer, accordingly. Besides the antiferromagnetic signal, the scattered intensity probed at the peak maximum position contains a background signal caused by specular reflectivity. This background is not expected to be affected by pumping. Since we did not determine the reflectivity background for every delay scan we underestimate the pump effect for the antiferromagnetic case slightly. This is illustrated in Fig. S1 C.

FERROMAGNETIC SIGNAL

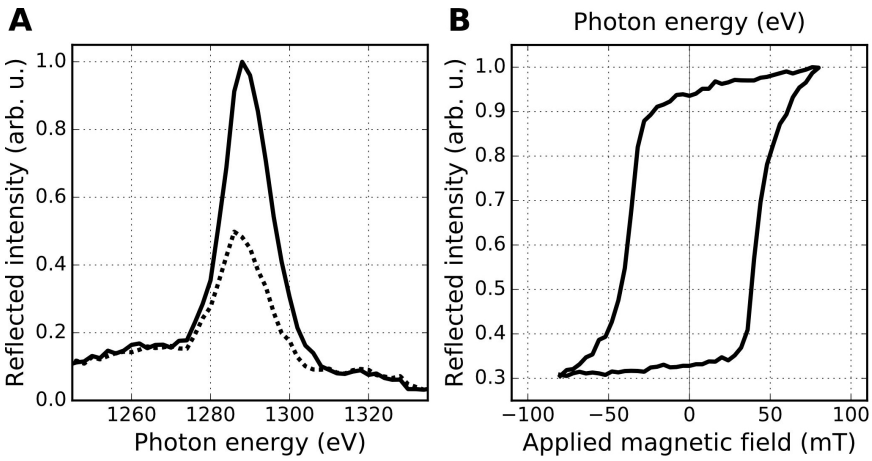

FIG. S2: Magnetic circular dichroism (MCD) in reflection. (A) X-ray reflection spectrum of the Dy M_5-edge in the ferromagnetic phase recorded with circularly polarized x-rays for opposite magnetization directions (solid and dashed line). (B) Magnetic hysteresis measured at a fixed photon energy of 1286 eV.

In the ferromagnetic phase we recorded the difference in specular reflected intensity at the Dy M_5 resonance for different relative orientations of magnetization and x-ray helicity, which is proportional to the magnetization [2]. The magnitude of the magnetic circular dichroism in reflection geometry depends on the incidence angle. We chose an incidence angle of 5 degrees, at which we reach large magnetic contrast with high overall intensity (Fig. S2 A). To magnetize the sample a static magnetic field of 80 mT was applied alternating between essentially parallel and antiparallel orientation with respect to the fixed x-ray helicity vector (in-plane magnetization). The magnetic hysteresis measured with this field geometry is shown in the Fig. S2 B.

LONG EXPONENTIAL TIME CONSTANTS

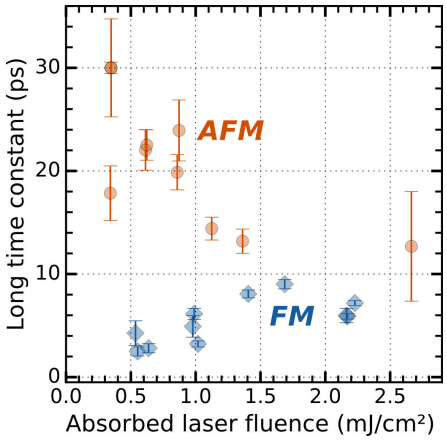

FIG. S3: Long exponential time constants extracted via the least-square fits as shown in Fig. S3&S4. We determined an average slow exponential time constant of (22 ± 7) ps for the antiferromagnetic (orange circles) and a single time constant of (6 ± 2) ps for the ferromagnetic phase (blue diamonds).

DATA ACQUISITION AND TREATMENT

The x-ray photons from the sample were detected with an avalanche photodiode (APD, Laser-Component SAR3000) operated close to the breakthrough voltage. This allowed us to use single photon counting detection. The APD is screened from the laser light by a 250 nm thick aluminum membrane which is attached to the light tight aluminum housing of the APD. Besides the dynamic magnetic signal with $\approx$ 100 fs temporal resolution, the raw detector signal contains background contributions from the halo background of the x-ray slicing source. The halo background is a consequence of the repetitive excitation of an identical electron bunch from the storage ring by the slicing process [3]. This results in an x-ray radiation background pulse with 70 ps duration. For the present experiment the ratio between halo and femtosecond x-ray intensity was typically 1/10 for linear polarization and 1/5 for elliptical polarization. To reliably eliminate the halo background from the data we directly measured exclusively the delay dependent transient of the halo background without the fs-x-ray pulses [4] for the pumped and the unpumped sample. The halo contribution (which also contains possible other background contributions due to dark counts in the detector or due to electronic noise) is then subtracted from the transient signal recorded with

the femtosecond x-ray pulses yielding the background-free *pumped* and *unpumped* signals that we used for the quantitative analysis (Fig. S4).

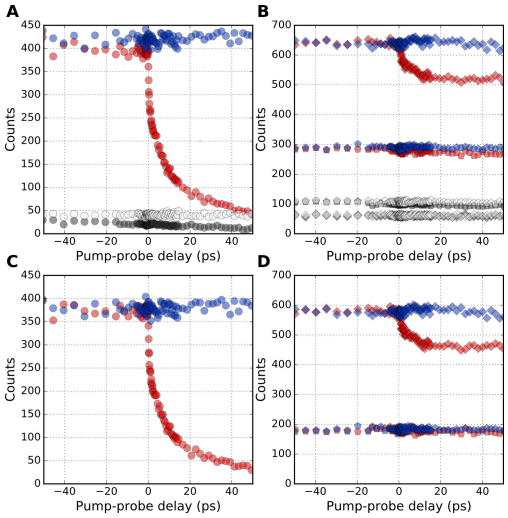

FIG. S4: Raw data and background subtraction. (A) & (B) Summed up raw data for a set of delay scans for a particular pump fluence (1 mJ/cm^2). The *pumped* signal is denoted with red and the *unpumped* signal with blue symbols. The respective halo backgrounds are the dark grey symbols (pumped) and light grey symbols (unpumped). Plot (A) exhibits the raw data for the antiferromagnetic case and (B) for the ferromagnetic case. In the latter the diamonds denote positive and the pentagons negative magnetization direction. (C) & (D) Respective delay scans after background subtraction.

DATA ANALYSIS

For both magnetic phases we recorded the *pumped* delay traces, the corresponding *unpumped* signal and the respective halo background. Figures S4 A&B show raw data for 1 mJ/cm^2 absorbed laser fluence. After background subtraction (Fig. S4 C&D) the signal proportional to the amount of magnetic order for a given delay is calculated for the antiferromagnetic case as

$$S_{\mathrm{AFM}} = \sqrt{\frac{S^p}{S^u}} \tag{2}$$

where S^p and S^u are background corrected *pumped* and *unpumped* signal, respectively. For the measurements in the ferromagnetic case the signal providing the amount of magnetic order is calculated as

$$S_{\mathrm{FM}} = \frac{\left(\overline{S^u} + S^p - S^u\right)^- - \left(\overline{S^u} + S^p - S^u\right)^+}{\overline{S^u}^- - \overline{S^u}^+} \tag{3}$$

Here, $\overline{S^u}$ is the delay-scan averaged *unpumped* signal. The antiferromagnetic transient signal $F_{\mathrm{AFM}}(t)$ is fitted by a double exponential decay function yielding two exponential time constants (f=fast, s=slow) convoluted by a Gaussian function to account for the temporal resolution (FWHM):

$$F_{\mathrm{AFM}}(t) = f_{\mathrm{AFM}}(t) \otimes \mathrm{Gauss}(\Delta t) \tag{4}$$

with

$$f_{\mathrm{AFM}}(t) = \begin{cases} I_0 & , t \leq t_0, \\ I_0 - I_f \left(1 - e^{-\frac{t-t_0}{\tau_f}}\right) & \\ -I_s \left(1 - e^{-\frac{t-t_0}{\tau_s}}\right) & , t > t_0. \end{cases} \tag{5}$$

The ferromagnetic dynamics were fitted by a single exponential decay function,

$$f_{\mathrm{FM}}(t) = \begin{cases} I_0 & , t \leq t_0, \\ I_0 - I_s \left(1 - e^{-\frac{t-t_0}{\tau_s}}\right) & , t > t_0. \end{cases} \tag{6}$$

again convoluted by a Gaussian function.

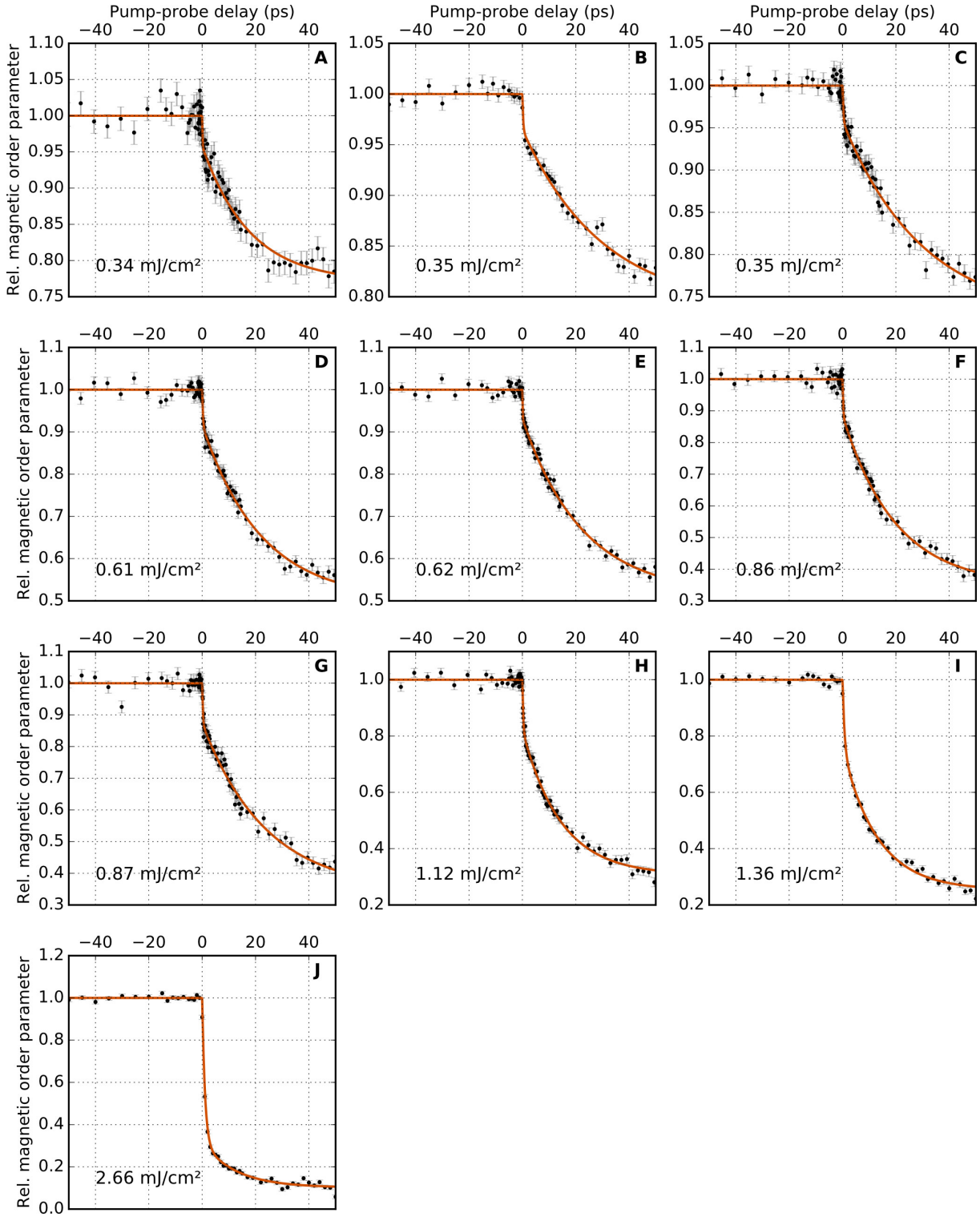

FIG. S5: Pump probe delay scans for antiferromagnetic order. For the relative order parameter the average signal at negative delay is normalized to 1. The error bars correspond to the one-σ standard deviation determined at negative delay. The solid lines denote the results of the fit analysis as described above.

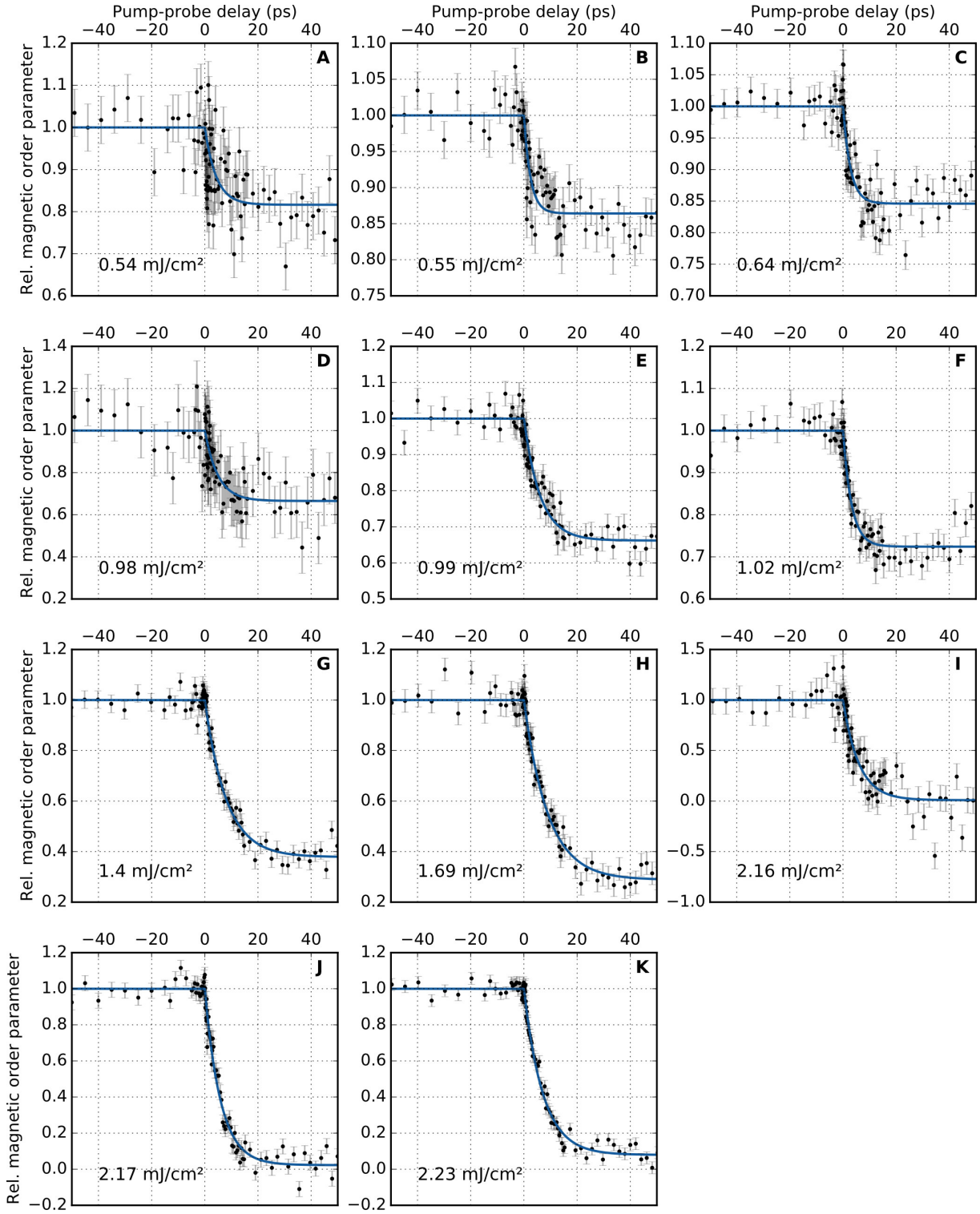

FIG. S6: Pump probe delay scans for ferromagnetic order. For the relative order parameter the average signal at negative delay is normalized to 1. The error bars correspond to the one-σ standard deviation determined at negative delay. The solid lines denote the results of the fit analysis as described above.

STATISTICAL ANALYSIS

All pump-probe delay scans for either the ferromagnetic or antiferromagnetic signals at a given pump fluence were normalized such that the average signal at negative delay was 1. The error bars in Fig. S5 & S6 correspond to the one-σ standard deviation of the data points at this negative delay. We verified that the such determined error bars were of the same size as when determined from counting statistics. All other quantities including parameter errors were derived from least-squares fits to the data. The fitting was performed with the lmfit package [5]. After having verified, that t_0 did not change between the experiments in the ferromagnetic and antiferromagnetic phase, we analyzed the data with t_0 fixed to a value determined from pump-probe delay scans performed at high laser fluences, where this quantity can be determined most accurately.

ANGULAR MOMENTUM TRANSFER RATE

As momentary angular momentum transfer rate we define the change of magnetic order parameter per time, hence the rate of transfer of angular momentum out of the ordered $4f$ spin system. We determined the angular momentum transfer rate from the fits to the delay scans by deriving them and scaling them to the magnitude of the equilibrium order parameter $M(T)$ at the particular sample temperature T. From Ref. 6 we inferred an ordered $4f$ magnetic moment of 9.84 μB at 40 K and 8.61 μB at 110 K. The maximum angular momentum transfer rate is the maximum change of magnetic order parameter for all pump-probe delays.

PUMP FLUENCE DETERMINATION

The pump laser fluence given in the present study is the absorbed fluence taking into account footprint effect and surface reflectivity. The pump laser pulse energy is determined from the laser power immediately before the laser is coupled into the vacuum chamber of the experiment. The laser spot size on the sample is experimentally determined in situ by scanning a 50-μm pinhole through the laser beam at the sample position. The pump laser reflectivity from the sample surface was determined experimentally as well (see Fig. S7).

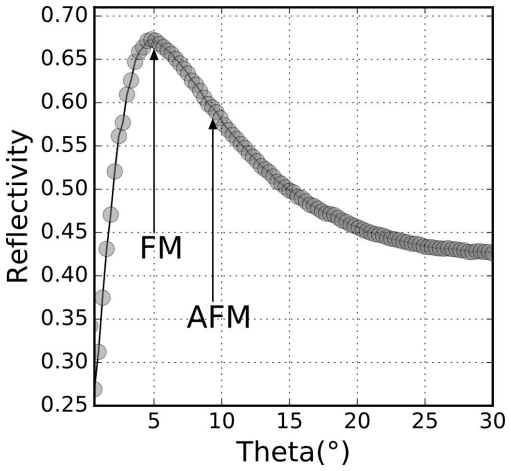

FIG. S7: Surface reflectivity from the Dy sample of the 800 nm pump-laser beam as a function of incidence angle θ. The arrows indicate the angles at which the time-resolved x-ray measurements were carried out for the ferromagnetic and antiferromagnetic case, respectively. The corresponding pump-laser-reflectivity values were used for determining the absorbed laser fluence. The drop off of reflected intensity for shallow angles below ≈ 7 degrees is a consequence of the projected laser beam spot which is getting larger than lateral dimensions of the sample leading to part of the laser beam missing the sample.

The footprint effect due to the grazing incidence enters by the factor $1/\sin\theta$. The absorbed laser fluence is then calculated as

$$F_l = \frac{P}{AR}\sin\theta(1-r) \tag{7}$$

where P is the laser power, R the repetition rate, A the laser cross section at the sample position, θ the scattering angle and r the relative reflectivity (Fig. S7). For measurements with varying scattering angle θ, the laser power P was adapted for every data point to

compensate a change of the factor $\sin\theta(1-r)$ such that the absorbed fluence F_l was kept at a constant value.

All plots in the Manuscript and the Supplementary Materials were created with the matplotlib Python package [7].

* Electronic address: nele.thielemann@helmholtz-berlin.de

[1] H. Ott, C. Schüßler-Langeheine, E. Schierle, A. Grigoriev, V. Leiner, H. Zabel, G. Kaindl, and E. Weschke, Phys. Rev. B **74**, 094412 (2006), ISSN 1098-0121, URL `http://link.aps.org/doi/10.1103/PhysRevB.74.094412`.

[2] H.-C. Mertins, D. Abramsohn, A. Gaupp, F. Schäfers, W. Gudat, O. Zaharko, H. Grimmer, and P. M. Oppeneer, Phys. Rev. B **66**, 184404 (2002), ISSN 0163-1829.

[3] K. Holldack, J. Bahrdt, A. Balzer, U. Bovensiepen, M. Brzhezinskaya, A. Erko, A. Eschenlohr, R. Follath, A. Firsov, W. Frentrup, et al., J. Synchrotron Radiat. **21**, 1090 (2014), ISSN 1600-5775.

[4] D. Schick, L. Le Guyader, N. Pontius, I. Radu, T. Kachel, R. Mitzner, T. Zeschke, C. Schüßler-Langeheine, A. Föhlisch, and K. Holldack, J. Synchrotron Radiat. **23**, 700 (2016), ISSN 1600-5775.

[5] M. Newville, T. Stensitzki, D. Allen, and A. Ingargiola, *LMFIT: Non-Linear Least-Square Minimization and Curve-Fitting for Python* (2014).

[6] M. K. Wilkinson, W. C. Koehler, E. O. Wollan, and J. W. Cable, J. Appl. Phys. **32**, S48 (1961), ISSN 0021-8979.

[7] M. Droettboom, J. Hunter, T. A. Caswell, E. Firing, P. Elson, D. Dale, J. H. Nielsen, B. Root, J.-J. Lee, J. K. Seppänen, et al. (2015).